

AD-A271 369



REPORT DOCUMENTATION PAGE

Form Approved
OMB No. 0704-0188

tion is estimated to average 1 hour per response, including the time for reviewing instructions, searching existing data sources, gathering and reviewing the collection of information, sending comments regarding this burden estimate or any other aspect of this burdening, to Washington Headquarters Services, Directorate for Information Operations and Reports, 1215 Jefferson Avenue, S.W., Washington, D.C. 20540, and to the Office of Management and Budget, Paperwork Reduction Project (0704-0188), Washington, D.C. 20503.

2. REPORT DATE
23 Aug 93

3. REPORT TYPE AND DATES COVERED
Technical

4. TITLE AND SUBTITLE

Thermomechanical and Magnetohydrodynamic Stability in Shaped-Charge Jets

5. FUNDING NUMBERS

① AA03-92-K-0005

6. AUTHOR(S)

David L. Littlefield

7. PERFORMING ORGANIZATION NAME(S) AND ADDRESS(ES)

Southwest Research Institute
P.O. Drawer 28510
San Antonio, TX 78238

DTIC
ELECTE
OCT 21 1993

8. PERFORMING ORGANIZATION REPORT NUMBER

9. SPONSORING / MONITORING AGENCY NAME(S) AND ADDRESS(ES)

U.S. Army Research Office
P. O. Box 12211
Research Triangle Park, NC 27709-2211

10. SPONSORING / MONITORING AGENCY REPORT NUMBER

ARO 30539.1-E6

11. SUPPLEMENTARY NOTES

The view, opinions and/or findings contained in this report are those of the author(s) and should not be construed as an official Department of the Army position, policy, or decision, unless so designated by other documentation.

12a. DISTRIBUTION / AVAILABILITY STATEMENT

Approved for public release; distribution unlimited.

12b. DISTRIBUTION CODE

13. ABSTRACT (Maximum 200 words)

In this study the stability characteristics of shaped-charge jets when exposed to axial electric currents are investigated. The objective of this study is to expand the results of previous analyses by Littlefield^{4,9} to include high levels of electric current, where thermal energy effects must be included. Coupling of the magnetohydrodynamic and thermal characteristics of the flow is accomplished solely through the variation of mechanical, thermal and electrical properties with temperature. Phase change effects are also included. The jet is assumed incompressible and perfectly plastic, with the Levy-von Mises criterion imposed to limit the effective stress. A linear variation of the effective stress with temperature is employed to simulate effects of thermal softening. Electrical resistivity and specific heat are permitted to vary linearly with temperature, coupled with associated jump values that occur as the jet changes phase. Solutions to the appropriate base flow are subjected to small axisymmetric disturbances, and linear perturbation theory is employed to determine the time evolution of these disturbances. Perturbations that grow the fastest in magnitude as time progresses are identified as the most unstable. Results of the analysis indicate that thermal effects can dramatically alter both the base and perturbed flow fields, as well as the growth rate of perturbations.

14. SUBJECT TERMS

Shaped-charge Jet, Stability, Magnetohydrodynamics, Plasticity.

15. NUMBER OF PAGES
10

16. PRICE CODE

17. SECURITY CLASSIFICATION OF REPORT
UNCLASSIFIED

18. SECURITY CLASSIFICATION OF THIS PAGE
UNCLASSIFIED

19. SECURITY CLASSIFICATION OF ABSTRACT
UNCLASSIFIED

20. LIMITATION OF ABSTRACT
UL

NSN 7540-01-280-5500

Standard Form 298 (Rev. 2-89)
Prescribed by ANSI Std. Z39-18
298-102

93 10 18 090

93-24804



THERMOMECHANICAL AND MAGNETOHYDRODYNAMIC STABILITY IN SHAPED-CHARGE JETS

by

David L. Littlefield

Southwest Research Institute
Engineering and Materials Sciences Division
P.O. Drawer 28510
San Antonio, TX 78228-0510
USA

In this study the stability characteristics of shaped-charge jets when exposed to axial electric currents are investigated. The objective of this study is to expand the results of previous analyses by Littlefield^{4,9} to include high levels of electric current, where thermal energy effects must be included. Coupling of the magnetohydrodynamic and thermal characteristics of the flow is accomplished solely through the variation of mechanical, thermal and electrical properties with temperature. Phase change effects are also included. The jet is assumed incompressible and perfectly plastic, with the Levy-von Mises criterion imposed to limit the effective stress. A linear variation of the effective stress with temperature is employed to simulate effects of thermal softening. Electrical resistivity and specific heat are permitted to vary linearly with temperature, coupled with associated jump values that occur as the jet changes phase. Solutions to the appropriate base flow are subjected to small axisymmetric disturbances, and linear perturbation theory is employed to determine the time evolution of these disturbances. Perturbations that grow the fastest in magnitude as time progresses are identified as the most unstable. Results of the analysis indicate that thermal effects can dramatically alter both the base and perturbed flow fields, as well as the growth rate of perturbations.


I. INTRODUCTION

Shaped-charge jets are one of the most effective anti-armor weapons in application today. Because of their superior penetrating ability, shaped charges are widely used as warheads by all branches of the military. The penetration capability results from the high velocities achieved by the jet tip, and from the long length facilitated by the axial velocity gradient. However, penetration performance of the shaped charge does have its limitations because after a specified time (the *breakup time*), the jet will particulate into many fragments roughly equal in size and begin to disperse. The penetrating ability of the jet is severely degraded after this occurs.

The particulation and breakup phenomenon observed in shaped charges suggested that the stretching motion of the jet may be unstable, and has prompted a number of experimental and theoretical investigations. Recent two dimensional analyses by Curtis¹, Pack², Romero³ and Littlefield^{4,9} have been successful in reproducing some of the behavior observed in experiments, indicating that the fragments formed after particulation should have lengths roughly on the order of the jet diameter. Perturbation studies were also extrapolated in order to estimate jet breakup times.

Recent theoretical studies have examined mechanisms by which the naturally-occurring instabilities in shaped-charge jets might be enhanced in order to promote premature breakup. Once demonstrated, these mechanisms would have the potential for incorporation into armor packages. One mechanism investigated originally by Walker⁹ involves the passage of an axial electric current through the jet. Although this technique was originally intended as a means to vaporize the jet, it later became apparent that axial currents could be used to promote the formation of instabilities similar to those seen in ideal plasma columns. This mechanism and others has been investigated by Toepfer¹⁰ and other researchers. Previous analyses by Littlefield^{4,9} have demonstrated that axial electric currents can be used to increase the growth

DTIC QUALITY INSPECTED 2

Dist	Special
A-1	

rate of instabilities, even when small currents are employed. The objective of this study is to expand the results from the previous research to include high levels of electric current, where thermal energy transfer mechanisms become important.

A number of assumptions have been made to make the analysis tractable yet retain as realistic conditions as possible. The jet is assumed to be incompressible, infinitely long, uniformly elongating, and perfectly plastic. An axial electric current initially on the surface of the jet is applied at time $t = 0$, and permitted to diffuse with time. This electric current produces an azimuthal magnetic field, which interacts with the current to produce Lorentz forces. The current also results in Joule heating, increasing the internal energy of the jet. Small disturbances to the idealized uniform jet motion are considered, and linear perturbation theory is employed to establish the equations governing the time evolution of these disturbances. The stability of the jet is determined from solutions to these equations.

The arrangement of this paper may be described approximately as follows. In Sec. II, the mathematical model and governing equations are presented. Solutions to these equations for the idealized motion of the jet are given in Sec. III. In Sec. IV, linear perturbation theory is used to develop the governing equations for small disturbances to the idealized jet motion. In Sec. V solutions to the perturbation equations are presented and discussed. Finally, Sec. VI contains some general comments and conclusions.

II. MODEL AND GOVERNING EQUATIONS

Consider a uniformly extending, perfectly plastic shaped-charge jet as is shown in Fig. 1. The radius at an arbitrary point along the jet boundary is denoted as $r_b(z, t)$, and the outward unit normal vector at this point as \mathbf{n} . An axial electric current $I(t)$, assumed to be supplied by an external power source, is applied at time $t = 0$. In this analysis the current is assumed constant, but it is a straightforward extension to augment the model for the case of arbitrary currents that can vary with time.

Let the velocity be given by \mathbf{V} , its components by v_i , the pressure by p , the deviatoric stress tensor by τ_{ij} , the current density by \mathbf{J} , the magnetic field by \mathbf{B} , the enthalpy by h , the temperature by T , the density by ρ , the magnetic permeability by μ_0 , the resistivity by λ , the specific heat by c_p , the thermal conductivity by k , and the yield strength by Y . Then the governing equations in the jet and in the surrounding vacuum are given by

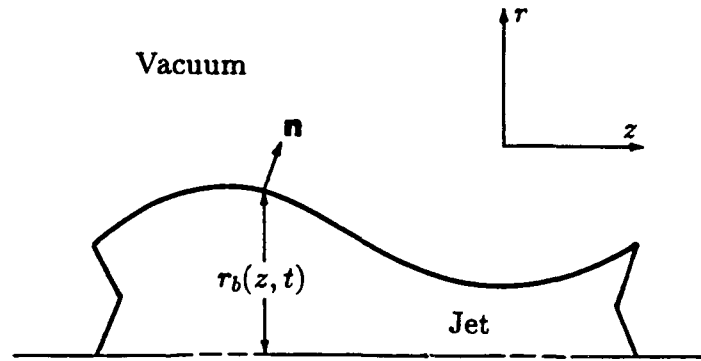


Fig. 1. Model for Jet Stability Calculations.

$$\rho \nabla \cdot \mathbf{V} = 0, \quad (1)$$

$$\rho \left(\frac{\partial \mathbf{V}}{\partial t} + \mathbf{V} \cdot \nabla \mathbf{V} \right) = -\nabla p + \nabla \cdot \tau_{ij} + \mathbf{J} \times \mathbf{B}, \quad (2)$$

$$\rho \left(\frac{\partial h}{\partial t} + \mathbf{V} \cdot \nabla h \right) = \frac{\partial p}{\partial t} + \mathbf{V} \cdot \nabla p + \lambda (\mathbf{J} \cdot \mathbf{J})^2 + \nabla \cdot (k \nabla T) + \tau_{ij} \frac{\partial v_i}{\partial x_j}, \quad (3)$$

$$\mathbf{E} + \mathbf{V} \times \mathbf{B} = \lambda \mathbf{J}, \quad (4)$$

$$\nabla \cdot \mathbf{B} = 0, \quad (5)$$

$$\nabla \times \mathbf{B} = \mu_0 \mathbf{J}, \quad (6)$$

and

$$\nabla \times \mathbf{E} = -\frac{\partial \mathbf{B}}{\partial t}. \quad (7)$$

Equations (1) - (3) are the incompressible continuity, momentum and energy equations, respectively; Eq. (4) is Ohm's law, and Eqs. (5) - (7) are Maxwell's equations. Several other relationships are needed to obtain closure. The temperature and enthalpy are related by

$$\frac{\partial h}{\partial T} = c_p, \quad (8)$$

and the constitutive model assumed for the jet is a perfectly plastic model, with the effective stress satisfying the von Mises criterion. The deviatoric stress depends only on the velocity and the yield strength under these conditions, and may be expressed as

$$\tau_{ij} = \mu \left(\frac{\partial v_i}{\partial x_j} + \frac{\partial v_j}{\partial x_i} \right), \quad (9)$$

where μ is a scalar that satisfies

$$\tau_{ij} \tau_{ij} = \frac{2Y^2}{3}. \quad (10)$$

Assuming the physical properties are known, Eqs. (1) - (8) when cast in cylindrical coordinates represent a system of 10 scalar equations for 10 scalar unknowns: v_r , v_z , p , E_r , E_z , J_r , J_z , B_θ , h , and T .

When large changes in thermal energy occur, several of the physical properties that appear in Eqs. (1) - (10) can change their values by several orders of magnitude. The changes must be considered in order to make accurate predictions of the jet motion. In the present study Y , k , c_p , λ were all permitted to vary with temperature according to the relationship

$$f = \begin{cases} \beta_1 + \beta_2 T & T < T_m \\ \beta_3 + \beta_4 T & T \geq T_m \end{cases}, \quad (11)$$

where the β_i 's are constants, T_m is the melting temperature and f is the specified physical property. In the phase change regime, properties were linearly interpolated as a function of enthalpy from their values at incipient to total melt. Variations of properties with respect to other state variables, such as pressure or equivalent plastic strain, were not considered. Although the density certainly changes with temperature, its variation is not as significant as with the other properties considered in this analysis. Furthermore, the inclusion of variable density complicates the analysis considerably and will therefore be deferred to future study.

Several of the physical properties listed in Eqs. (1) - (10) are discontinuous at the interface between the jet boundary and the surrounding vacuum. The density, for instance, changes suddenly from its value in the jet to zero in the surrounding vacuum. The procedure for treating this boundary that insures the conservation equations are still satisfied is to integrate Eqs. (1) - (10) across a layer of thickness δ in a direction normal to the boundary, and then allow δ to approach zero¹¹. This procedure yields the correct boundary conditions, which are given by

$$v_r = \frac{\partial r_b}{\partial t} + \mathbf{V} \cdot \nabla r_b, \quad (12)$$

$$-\mathbf{n} \cdot [\mathbf{p}] + \mathbf{n} \cdot [\tau_{ij}] = 0, \quad (13)$$

$$\mathbf{n} \cdot [k \nabla T] - \mathbf{n} \cdot [\mathbf{V} \mathbf{p}] + \mathbf{n} \cdot [\mathbf{V} \cdot \tau_{ij}] = 0, \quad (14)$$

$$\mathbf{n} \cdot [\mathbf{B}] = 0, \quad (15)$$

and

$$\mathbf{n} \times [\mathbf{E}] = -\mathbf{n} \cdot \mathbf{v}[\mathbf{B}], \quad (16)$$

where $[\]$ denotes the change in the specified quantity across the boundary, and \mathbf{v} is the velocity of the boundary. The outward unit normal vector \mathbf{n} may be determined as

$$\mathbf{n} = \frac{\nabla(r - r_b)}{|\nabla(r - r_b)|}. \quad (17)$$

Equations (1) - (10), together with the boundary conditions given in Eqs. (12) - (17), represent a system of coupled differential equations to calculate the time evolution of the jet motion. In their most general form, this set of equations is formidable and quite difficult to solve. However, simplified solutions which examine the stability of the idealized motion of the jet may be performed with a reduced set of equations. Solutions to this reduced set of equations allow easier identification of the physical principles that contribute to the instability and breakup of shaped-charge jets.

III. IDEALIZED MOTION OF THE JET

In the idealized motion of a shaped-charge jet, the jet stretches uniformly with constant tip and tail velocities V_{tip} and V_{tail} . The axial strain rate η is therefore $\eta = (V_{tip} - V_{tail})/L$, where L is the instantaneous length of the jet. Since L increases as time progresses, η decreases. When cast in a reference frame that moves with the center of mass, so that $v_z = 0$ and $z = 0$ at the mass center, these kinematic considerations yield a velocity distribution given by

$$v_{z0} = \eta z; \quad v_{r0} = -\eta r/2, \quad (18)$$

where the subscript 0 denotes the idealized motion of the jet. Similarly, the length and axial strain rate are given by

$$\eta = \eta_0/\tau; \quad L = L_0\tau, \quad (19)$$

where the subscript 0 denotes initial values and $\tau = 1 + \eta_0 t$. The pressure, enthalpy and magnetic field in the jet are determined by solving appropriate conservation equations. These variables may be cast in dimensionless form by letting $\bar{p}_0 = 4\pi^2 a^2 p_0 / \mu_0 I^2$, $\bar{h}_0 = h_0 / h_m$, $\bar{T}_0 = (T_0 - T_o) / (T_m - T_o)$, $\bar{B}_0 = 2\pi a B_0 / \mu_0 I$, and $\bar{r} = r\sqrt{\tau}/a$, where a is the initial radius, I is the electric current, h_m is the enthalpy at melting, and B is the azimuthal component to \mathbf{B} . Use of these dimensionless variables in the governing equations yields

$$\Lambda \frac{\partial \bar{p}_0}{\partial \bar{r}} + \frac{3\bar{r}}{4\tau^3} + \frac{1}{\Omega} \frac{\partial \bar{Y}_0}{\partial \bar{r}} + \Lambda \bar{B}_0 \left(\frac{\partial \bar{B}_0}{\partial \bar{r}} + \frac{\bar{B}_0}{\bar{r}} \right) = 0, \quad (20)$$

$$\frac{\partial \bar{h}_0}{\partial \tau} - E\Lambda \frac{\partial \bar{p}_0}{\partial \tau} - \frac{E\Lambda}{R} \tau \bar{\lambda}_0 \left(\frac{\partial \bar{B}_0}{\partial \bar{r}} + \frac{\bar{B}_0}{\bar{r}} \right)^2 - \frac{3\tau}{P\Omega \bar{r}} \frac{\partial}{\partial \bar{r}} \left(\bar{k}_0 \bar{r} \frac{\partial \bar{T}_0}{\partial \bar{r}} \right) = 0, \quad (21)$$

and

$$\frac{\partial \bar{B}_0}{\partial \tau} + \frac{\bar{B}_0}{2\tau} - \frac{\tau}{R} \frac{\partial}{\partial \bar{r}} \left[\bar{\lambda}_0 \left(\frac{\partial \bar{B}_0}{\partial \bar{r}} + \frac{\bar{B}_0}{\bar{r}} \right) \right] = 0, \quad (22)$$

where $\bar{Y}_0 = Y_0/Y(T_o)$, $\bar{\lambda}_0 = \lambda_0/\lambda(T_o)$, and $\bar{k}_0 = k_0/k(T_o)$. Plastic work has been neglected in this formulation because it is small for the problem at hand. The dimensionless constants appearing in these equations are

$$\Omega = \frac{3\rho\eta_o^2 a^2}{Y(T_o)}; \quad \Lambda = \frac{\mu_o I^2}{4\pi^2 \rho \eta_o^2 a^4}; \quad P = \frac{c_p(T_o) \left(1 + \frac{c_1}{2}\right)}{k(T_o)\eta_o};$$

$$E = \frac{\eta_o^2 a^2}{h_m}; \quad R = \frac{\mu_o \eta_o a^2}{\lambda(T_o)};$$

where c_p is the slope of the specific heat-temperature curve for the solid. Physically, Ω represents a ratio of inertial to plastic forces, Λ a ratio of electromagnetic to inertial forces, P a ratio of "plastic" to thermal diffusion, E a ratio of kinetic energy to sensible heat, and R a ratio of magnetic convection to diffusion. Furthermore, when the physical properties are cast in dimensionless form using Eq. (10), two additional constants arise and are given by

$$S = \frac{h_m}{h_{lp}}; \quad Q = \frac{h_v}{h_m};$$

where h_{lp} is the latent heat of fusion and h_v is the enthalpy at vaporization.

Boundary and initial conditions are required to solve Eqs. (20) - (22). The boundary conditions are determined from the conditions in Eqs. (11)- (17), which yield

$$\bar{p}_0 = -\frac{\bar{y}_0}{\Omega}; \quad \bar{k}_0 \frac{\partial \bar{T}_0}{\partial \bar{r}} = 0; \quad \bar{B}_0 = \sqrt{\tau}; \quad (23)$$

and are evaluated at $\bar{r} = 1$. Initially the jet was assumed to be isothermal with no electric current flowing, so \bar{p}_0 , \bar{h}_0 , and \bar{B}_0 were all set to zero at $\tau = 1$.

Shown in Fig. 2 is the dimensionless temperature, pressure and magnetic field distribution as a function of normalized radius in the jet at three different times. The parameter Λ was chosen as 100, whereas the remaining parameters were assigned values typical for shaped-charge jets, and are listed in Table 1. While at early times significant surface heating occurs, central portions of the jet begin to rise in temperature at later times. This body heating is a result of the temperature variation in resistivity, which causes the current density to rise in the center of the jet where the resistance is lower. The net result is a quasi-uniform temperature distribution so that the entire cross section of the jet melts almost simultaneously.

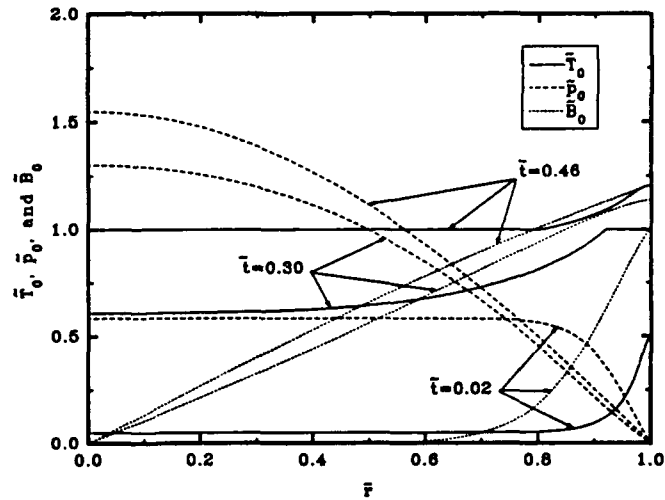


Fig. 2. Normalized Temperature, Pressure and Magnetic Field Distribution vs. Normalized Radius.

In the vacuum surrounding the jet, the governing equations presented in the previous section are all identically satisfied except for Eqs. (5) and (6). Furthermore, since $\mathbf{J} \equiv 0$ in the vacuum, these equations reduce to

$$\nabla^2 \bar{B}_0 = 0, \quad (24)$$

which yields the solution $\bar{B}_0 = \sqrt{\tau}/\bar{r}$.

Table 1. Numerical Values of Dimensionless Parameters

Ω	0.879
R	2.13
E	5.07×10^{-3}
P	2880
S	1.50
Q	4.02

IV. FIRST-ORDER EQUATIONS

Small axisymmetric disturbances to the uniform jet motion were then considered using perturbation analysis. Application of perturbation theory to the governing equations yields a set of linear partial differential equations that describe the time evolution of disturbances to the jet motion. Disturbances that continue to grow as time progresses are identified as unstable. The fastest growing instability is an indication of the most prevalent disturbance in the actual jet motion.

The algebraic details of the derivation for the perturbation equations are complicated and quite cumbersome, and for brevity will not be repeated here. The equations are formed by expanding the dependent variables in a Taylor series for ϵ , keeping only the terms are of order ϵ^1 . Furthermore, previous analysis has demonstrated that transformation of the governing equations into the lagrangian coordinates

$$\bar{r} = r\sqrt{\tau}/a; \quad \bar{z} = z/a\tau \quad (25)$$

permits the axial dependence of dependent variables to be Fourier analyzed. Let

$$\begin{aligned} v_{r1} &= \eta_o a \bar{v}_r \exp(ik\bar{z}); \\ v_{z1} &= \eta_o a \bar{v}_z \exp(ik\bar{z}); \\ p_1 &= \mu_o J^2 \bar{p} \exp(ik\bar{z})/4\pi^2 a^2; \\ h_1 &= h_m \bar{h} \exp(ik\bar{z}); \\ B_1 &= \mu_o J \bar{B} \exp(ik\bar{z})/2\pi a; \\ T_1 - T_o &= (T_m - T_o) \bar{T} \exp(ik\bar{z}); \\ Y_1 &= Y_o \bar{Y} \exp(ik\bar{z}); \\ \lambda_1 &= \lambda_o \bar{\lambda} \exp(ik\bar{z}); \\ k_1 &= k_o \bar{k} \exp(ik\bar{z}); \end{aligned} \quad (26)$$

where k is the axial wavenumber, $i = \sqrt{-1}$, and the 1 subscript denotes a first order quantity. Then the differential equations governing the motion of small disturbances are given by

$$\frac{\partial \bar{v}_r}{\partial \bar{r}} + \frac{\bar{v}_r}{\bar{r}} + \frac{ik}{\tau^{3/2}} \bar{v}_z = 0, \quad (27)$$

$$\begin{aligned} \frac{\partial \bar{v}_r}{\partial \tau} - \frac{\bar{v}_r}{2\tau} = & -\Lambda \tau^{1/2} \frac{\partial \bar{p}}{\partial \bar{r}} - \frac{1}{\Omega} \left[\frac{\bar{Y}_o}{\tau} k^2 \bar{v}_r + \tau^{1/2} \frac{\partial \bar{Y}}{\partial \bar{r}} - \tau^2 \frac{\partial \bar{Y}_o}{\partial \bar{r}} \left(\frac{\partial \bar{v}_r}{\partial \bar{r}} - \frac{\bar{v}_r}{\bar{r}} \right) \right] \\ & - \Lambda \tau^{1/2} \left[\bar{B} \frac{\partial \bar{B}_o}{\partial \bar{r}} + \bar{B}_o \frac{\partial \bar{B}}{\partial \bar{r}} + 2 \frac{\bar{B}_o \bar{B}}{\bar{r}} \right], \end{aligned} \quad (28)$$

$$\begin{aligned} \frac{\partial \bar{v}_z}{\partial \tau} + \frac{\bar{v}_z}{\tau} = & -\frac{\Lambda}{\tau} ik \bar{p} + \frac{\tau^2}{\Omega} \bar{Y}_o \left[\frac{\partial^2 \bar{v}_z}{\partial \bar{r}^2} + \frac{1}{\bar{r}} \frac{\partial \bar{v}_z}{\partial \bar{r}} + \frac{k^2}{\tau^3} \bar{v}_z \right] \\ & + \frac{1}{\Omega} \left[\frac{2ik}{\tau} \bar{Y} + \tau^{1/2} \frac{\partial \bar{Y}_o}{\partial \bar{r}} \left(ik \bar{v}_r + \tau^{3/2} \frac{\partial \bar{v}_z}{\partial \bar{r}} \right) \right] - \frac{ik\Lambda}{\tau} \bar{B}_o \bar{B}, \end{aligned} \quad (29)$$

$$\begin{aligned} \frac{\partial \bar{h}}{\partial \tau} + \tau^{1/2} \frac{\partial \bar{h}_o}{\partial \bar{r}} \bar{v}_r = & E\Lambda \left(\frac{\partial \bar{p}}{\partial \tau} + \tau^{1/2} \frac{\partial \bar{p}_o}{\partial \bar{r}} \bar{v}_r \right) + \frac{E\Lambda}{R} \tau \left[\bar{\lambda} \left(\frac{\partial \bar{B}_o}{\partial \bar{r}} + \frac{\bar{B}_o}{\bar{r}} \right)^2 \right. \\ & \left. + 2\bar{\lambda}_o \left(\frac{\partial \bar{B}_o}{\partial \bar{r}} + \frac{\bar{B}_o}{\bar{r}} \right) \left(\frac{\partial \bar{B}}{\partial \bar{r}} + \frac{\bar{B}}{\bar{r}} \right) \right] + \frac{3\tau}{P\Omega} \left[\frac{1}{\bar{r}} \frac{\partial}{\partial \bar{r}} \left(\bar{k} \bar{r} \frac{\partial \bar{T}_o}{\partial \bar{r}} \right) + \frac{1}{\bar{r}} \frac{\partial}{\partial \bar{r}} \left(\bar{k}_o \bar{r} \frac{\partial \bar{T}}{\partial \bar{r}} \right) - \frac{k^2}{\tau^3} \bar{k}_o \bar{T} \right], \end{aligned} \quad (30)$$

and

$$\begin{aligned} \frac{\partial \tilde{B}}{\partial \tau} + \tau^{1/2} \left(\frac{\partial \tilde{B}_0}{\partial \tilde{r}} - \frac{\tilde{B}_0}{\tilde{r}} \right) \tilde{v}_r = \frac{\tau}{R} \left[\tilde{\lambda}_0 \left(\frac{\partial^2 \tilde{B}}{\partial \tilde{r}^2} + \frac{1}{\tilde{r}} \frac{\partial \tilde{B}}{\partial \tilde{r}} - \frac{\tilde{B}}{\tilde{r}^2} - \frac{k^2}{\tau^3} \tilde{B} \right) \right. \\ \left. + \tilde{\lambda} \left(\frac{\partial^2 \tilde{B}_0}{\partial \tilde{r}^2} + \frac{1}{\tilde{r}} \frac{\partial \tilde{B}_0}{\partial \tilde{r}} - \frac{\tilde{B}_0}{\tilde{r}^2} \right) + \frac{\partial \tilde{\lambda}_0}{\partial \tilde{r}} \left(\frac{\partial \tilde{B}}{\partial \tilde{r}} + \frac{\tilde{B}}{\tilde{r}} \right) + \frac{\partial \tilde{\lambda}}{\partial \tilde{r}} \left(\frac{\partial \tilde{B}_0}{\partial \tilde{r}} + \frac{\tilde{B}_0}{\tilde{r}} \right) \right]. \end{aligned} \quad (31)$$

In the vacuum surrounding the jet, solutions to the first order equations require $\tilde{B} = 0$ in the vacuum. This result also follows directly from Ampere's law, since the total current enclosed by the jet does not change when an axisymmetric disturbance is applied.

Several boundary and initial conditions are required to solve Eqs. (26) - (30). The initial conditions have been presented elsewhere⁶ and are still valid in the present analysis if h_i is assumed zero initially. Calculations demonstrated that the initial value of h_i has a negligible effect on the results anyway, so in the present study the initial value of h_i was set to zero. The boundary conditions result from Eqs. (11) - (17), and are derived using a procedure similar to the one used to determine the governing perturbation equations. These conditions are given by

$$\frac{\partial \tilde{r}_b}{\partial \tau} - \tau^{1/2} \tilde{v}_r = 0, \quad (32)$$

$$\tilde{p} - \left[\frac{3}{4\Lambda\tau^3} + \tau^{1/2} \left(\frac{\partial \tilde{B}_0}{\partial \tilde{r}} + \tau^{1/2} \right) \right] \tilde{r}_b + \frac{1}{\Omega\Lambda} \left[\tilde{p} - \tilde{p}_0 \left(2\tau^{3/2} \frac{\partial \tilde{v}_r}{\partial \tilde{r}} + ik\tilde{v}_z \right) \right] = 0, \quad (33)$$

$$\frac{3ik}{\tau^{3/2}} \tilde{r}_b - ik\tilde{v}_r - \tau^{3/2} \frac{\partial \tilde{v}_z}{\partial \tilde{r}} = 0, \quad (34)$$

$$\tilde{B} + \left(\tau^{1/2} + \frac{\partial \tilde{B}_0}{\partial \tilde{r}} \right) \tilde{r}_b = 0, \quad (35)$$

and

$$\tilde{k}_0 \frac{\partial \tilde{T}}{\partial \tilde{r}} + \tilde{k} \frac{\partial \tilde{T}_0}{\partial \tilde{r}} + \tilde{k}_0 \frac{\partial^2 \tilde{T}_0}{\partial \tilde{r}^2} \tilde{r}_b = 0, \quad (35)$$

and are evaluated at $\tilde{r} = 1$. In these equations, the variable \tilde{r}_b is the amplitude of the disturbance to the radius of the jet, defined as

$$r_{b1} = a \tilde{r}_b \exp(ik\tilde{z})/\tau^{1/2}. \quad (37)$$

The numerical value of \tilde{r}_b has special significance since it is a dimensionless measure of the magnitude of perturbations to the jet boundary. Therefore, disturbances that maximize the value of \tilde{r}_b are readily identified as the most unstable perturbations.

V. SOLUTIONS TO PERTURBATION EQUATIONS AND STABILITY CHARACTERISTICS OF THE JET

Numerical solutions to the perturbation equations presented in Sec. IV were calculated for a wide range of electric currents and disturbance wavelengths. As a result of the lagrangian transformation applied to the governing equations, the wavelength is time dependent and related to the wavenumber as $\lambda_w = 2\pi a \tau / k$, so initially short wavelengths become longer and stretch at the same rate as the jet length. Large electric currents were applied in the model by increasing the value of the parameter Λ , in order to investigate the effects of large internal energy changes on the jet stability.

Shown in Fig. 3 is the normalized amplitude of the perturbed radius \bar{r}_b as a function of normalized time τ for several different wavelengths. The value of Λ was 1.0, and the values of the other dimensionless parameters were as given in Table 1. For this value of Λ , thermal effects are uncoupled from the momentum and magnetic fields since the maximum value of \bar{h}_0 reaches only 0.03 when $\tau = 1$. Consequently, the values of \bar{r}_b overlay almost exactly the values obtained from an isothermal model⁶, where energy balance effects were neglected. It is evident from the figure that disturbances corresponding to the wavenumber $k = \pi$ grow at the largest rate for most times. This wavenumber corresponds to an initial disturbance wavelength on the order of the jet diameter. Furthermore, disturbances grow faster than the case where no current is applied ($\Lambda = 0$). Extrapolation of this result to large amplitude disturbances would indicate that when low levels of electric current are applied, jets should particulate into fragments with lengths roughly equal to or slightly greater than the jet diameter.

The contribution of hydrodynamic and electromagnetic effects to instabilities in jets under isothermal conditions has been discussed at length elsewhere^{4,9}, and for brevity will be only summarily discussed here. The hydrodynamic instability results from an axial stress that opposes the stretching motion of the jet, which is positive and constant for the idealized jet motion. When combined with the reduction in cross-sectional area in regions where necking occurs, this constant axial stress results in a net force that always tends to accelerate material out of the neck, thus resulting in an unconditional instability. Moreover, in the absence of any stabilizing effects, this criterion would indicate that very short wavelength disturbances should be the most unstable. However, the short wavelength disturbances are partially stabilized by stress enhancement that occurs in the necking regions. The most unstable hydrodynamic disturbances, therefore, have moderate wavelengths. The electromagnetic contribution to the instability occurs because the axial current density tends to increase in the necked regions, resulting in an increase in magnetic pressure. This pressure increase also tends to accelerate material out of necking regions, and results in unconditional instability.

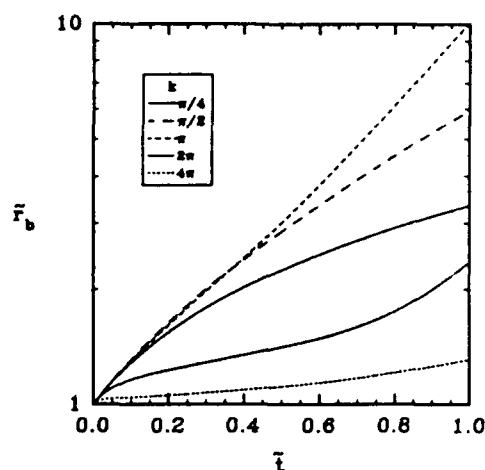


Fig. 3. Normalized amplitude \bar{r}_b vs. normalized time for several values of k . The value of Λ was 1.0, and the values of the other dimensionless parameters are given in Table 1.

When the electric current is increased, the behavior of instabilities in the jet change both in magnitude and character. Shown in Fig. 4 is the normalized amplitude of the perturbed radius as a function of normalized time for disturbances of several different wavenumbers. The value of Λ was 100, and the values of the other dimensionless parameters were as given in Table 1. For this value of Λ , incipient melt initiates at the surface at about $\tau = 0.2$, and complete melt begins to occur at $\tau = 0.45$. It is evident from the figure that larger currents result in dramatic increases in the growth rate of instabilities. Furthermore, the shortest wavelength disturbances appear to grow even faster when Λ is increased. When $\tau = 0.8$, for example, Fig. 4 indicates that disturbances corresponding to $k = 2\pi$ have the largest perturbed radius. This wavenumber corresponds to a wavelength equal to roughly half the jet diameter. Moreover, it is apparent from the slopes of \bar{r}_b that perturbations corresponding to $k = 4\pi$ grow at an even faster rate. This seems to indicate that the shortest wavelength perturbations will eventually become the most unstable disturbances.

The changes observed in the growth rate of \bar{r}_b when Λ is increased are a result of the additional importance of electromagnetic instabilities. As the current increases, the temperature increases and the jet material softens, until the yield strength is essentially zero at the melting point. Since hydrodynamic instabilities in the jet are a direct result of material strength, hydrodynamic effects do not contribute significantly to instability after incipient melting. The electromagnetic instabilities, on the other hand, become increasingly dominant. Furthermore, it is evident that the shortest wavelength disturbances should grow faster when electromagnetic instabilities are prevalent, since the axial magnetic pressure gradient that activates the instability becomes larger as the wavelength diminishes. This phenomenon is similar in nature to the electromagnetic instabilities seen in ideal plasma columns, where the shortest wavelength

disturbances possess the largest growth rates¹¹. Results in Figs. 3 and 4 are in qualitative agreement with this trend, indicating that the wavelength of the most unstable perturbation decreases with increasing current.

It is noteworthy to compare the results from the present analysis to the results when isothermal conditions are assumed. Shown in Fig. 5 is \bar{r}_b as a function of $\bar{\tau}$ at several wavenumbers calculated using an isothermal model⁶. The value of Λ was 100, and the remaining parameters are given in Table 1. A comparison of Figs. 4 and 5 indicates that the isothermal model underpredicts the late time growth rate of all disturbances, but particularly the short wavelength perturbations. This reduction in growth rate is a result of the absence of thermal softening in the isothermal model. Without thermal softening, the jet is partially stabilized by the axial stress enhancement that occurs in necked regions. Moreover, this stress enhancement effect increases in magnitude as the wavelength diminishes, which explains why the short wavelength disturbances are stabilized considerably when thermal softening is omitted. The magnitude of this stabilizing effect appears to be considerable and is indeed a surprising result, considering that the plastic forces were about two orders of magnitude smaller than the electromagnetic forces in this example.

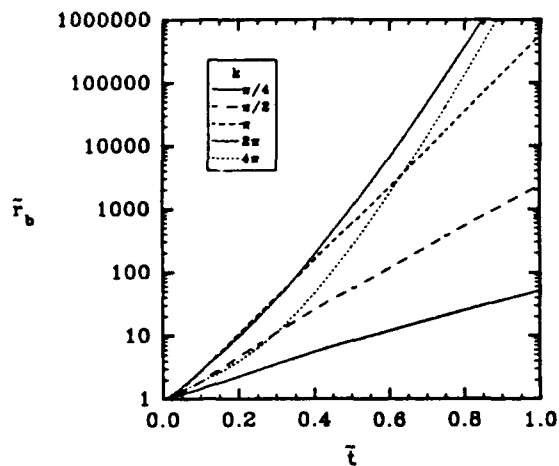


Fig. 4. Normalized amplitude \bar{r}_b vs. normalized time for several values of k . The value of Λ was 100, and the values of the other dimensionless parameters are given in Table 1.

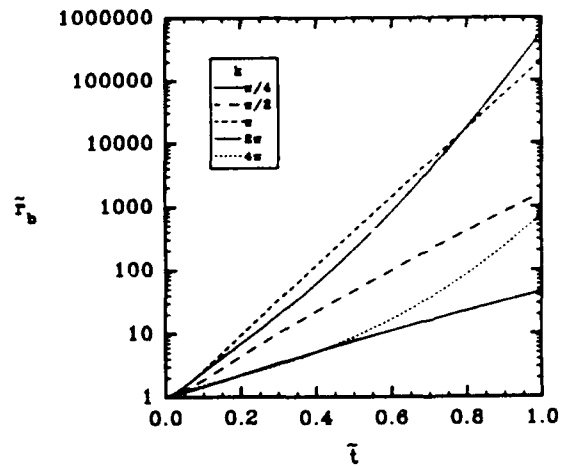


Fig. 5. Normalized amplitude \bar{r}_b vs. normalized time under isothermal conditions for several values of k . The value of Λ was 100, and the values of the other dimensionless parameters are given in Table 1.

VI. CONCLUSIONS

Large axial electric currents can have a powerful disrupting effect on shaped-charge jets. Results from the perturbation calculations indicate that growth rates in the perturbed radius can be increased by a factor of $10^4 - 10^5$ over their normal values when $\Lambda = 100$. Using typical numerical values for strain rate, radius and density in copper shaped-charge jets, $\Lambda = 100$ corresponds to an axial electric current of about 400 kA. Although this is a large electric current, it is definitely realizable and within the realm of existing pulsed-power technology.

ACKNOWLEDGEMENTS

This work was supported by the U. S. Army Research Office under Contract No. DAAL03-92-K-0005.

REFERENCES

1. Curtis, J. P., *Axisymmetric Model Instability Model for Shaped Charge Jets*, J. Appl. Phys. **61** (11), June 1987, pp. 4978 - 4985.
2. Pack, D. C., *On the Perturbation and Break Up of a High-Speed, Elongating Metal Jet*, J. Appl. Phys. **63** (6), March 1988, pp. 1864 - 1871.

3. Romero, L. A., *The Instability of Rapidly Stretching Plastic Jets*, J. Appl. Phys. **65** (8), April 1989, pp. 3006 - 3016.
4. Littlefield, D. L. and Powell, J. D., *The Effect of Electromagnetic Fields and the Stability of a Uniformly Elongating Plastic Jet*, Phys. Fluids A **2** (12), December 1990, pp. 2240 - 2248.
5. Littlefield, D. L. and Powell, J. D., *The Effect of Electromagnetic Fields on the Stability of a Perfectly Conducting Shaped-Charge Jet*, Proceedings, 12th International Symposium on Ballistics, November 1990, San Antonio, TX, pp. 359-368.
6. Littlefield, D. L., *Finite Conductivity Effects on the MHD Instabilities in Uniformly Elongating Plastic Jets*, Phys. Fluids A **3** (6), June 1991, pp. 166 - 1673.
7. Powell, J. D. and Littlefield, D. L., *Effect of Electromagnetic Fields on the Stability of a Perfectly Conducting, Axisymmetric Shaped-charge Jet*, BRL-TR-3108, U. S. Army Ballistic Research Laboratory, Aberdeen Proving Ground, MD, June 1990.
8. Littlefield, D. L., *The Effect of Finite Conductivity on MHD Instabilities in Axisymmetric Shaped-Charge Jets*, BRL-TR-3318, U. S. Army Ballistic Research Laboratory, Aberdeen Proving Ground, MD, March 1992.
9. Walker, E. H., *Defeat of Shaped-Charge Devices by Active Armor*, BRL-MR-2309, U. S. Army Ballistic Research Laboratory, Aberdeen Proving Ground, MD, 1973.
10. Toepfer, A. J., Ford, R., Parkinson, E. R., Rigby, F., Brown, R., and Wells, J., *Experiments on Electromagnetic Coupling to Scaled Rods (U)*, presented at 4th Annual TACOM Combat Vehicle Survivability Symposium, 31 March 1993.
11. Kruskal, M. and Schwartzschild, M., *Some Instabilities of a Completely Ionized Plasma*, Proc. Roy. Soc. **A223**, 1954, pp. 348 - 360.